A coupled 1D/3D simulation for the flow behaviour inside a close-coupled catalytic converter

Liu, Z. , Benjamin, S.F. , Roberts, C.A. , Zhao, H. and Arias-Garcia, A.

A Coupled 1D/3D Simulation for the Flow Behaviour inside a Close-Coupled Catalytic Converter

Z. Liu, S. F. Benjamin, C. A. Roberts, H. Zhao, A. Arias-Garcia

Coventry University

Notice about photocopy

In order to photocopy any works from this publication, you or your organization must obtain permission from the following organization which you has been delegated for copyright for clearance by the copyright owner of this publication.

Except in the U.S.A.
Japan Academic Association for Copyright Clearance   (JAACC)
6-41 Akasaka 9-chome, Minato-ku, Tokyo 107-0052   Japan
TEL: 81-3-3475-5618   Fax: 81-3-3475-5619   E-mail:naka-atsu@mju.biglobe.ne.jp

In the U.S.A.
Copyright Clearance Center, Inc.
222 Rosewood Drive, Danvers, MA 01923   U.S.A.
Phone: 1-978-750-8400   Fax:1-978-750-4744

A Coupled 1D/3D Simulation for the Flow Behaviour inside a Close-Coupled Catalytic Converter

Z. Liu, S. F. Benjamin, C. A. Roberts, H. Zhao and A. Arias-Garcia
Coventry University

ABSTRACT

This paper describes the coupling of a 1D engine simulation code (Ricardo WAVE) to a 3D CFD code (STAR-CD) to study the flow behaviour inside a Close-Coupled Catalytic converter (CCC). A SI engine was modelled in WAVE and the CCC modelled in STAR-CD. The predictions of the stand-alone WAVE model were validated against engine bed tests before the coupled 1D/3D simulations were performed at 3000 RPM WOT for both motored and firing conditions. The predicted exhaust velocities downstream of the catalyst monolith in the coupled simulations matched fairly well with Laser Doppler Anemometry (LDA) measurements.

INTRODUCTION

The ever more stringent legislation to reduce motor vehicle exhaust emissions has led to extensive research on the performance of catalytic converters. The flow field characteristics in the exhaust system are of particular interest, since they affect catalyst warm-up, light-off, life time, overall utilisation and conversion efficiency [1,2]. To reduce cold start emissions, converters have been moved from the traditional under body position to a close-coupled position near to the engine [3-5]. Understanding the complex internal flow of CCCs is required both to interpret their performance and to aid design optimisation.

Over the past decade or so, Computational Fluid Dynamics (CFD) models have been widely used to study the complicated 3D unsteady flow behaviour inside catalytic converters [6-8]. However, the transient boundary conditions of the CFD domain must be defined with reasonable accuracy for CFD models to give realistic predictions. Experimental methods can be used to measure the boundary conditions in a real engine environment, however they are time-consuming and costly. Consequently more researchers are utilising 1D gas dynamic and engine simulation codes to predict the transient

exhaust behaviour within the catalyst [9,10]. Such 1D engine simulations can be performed and the exhaust flux and state variables written to a file, which then provides 3D CFD models with the necessary boundary conditions [11,12]. However the real time mutual influence, between the 3D CFD model and 1D engine piping system, can only be established by performing a time-step based coupled simulation.

To date there have been few studies published in the open literature on the coupled simulation to investigate the flow characteristics within the exhaust system [13]. The work discussed here reports the coupling of a 1D engine simulation code to a 3D CFD code to investigate the flow behaviour inside a production CCC system, and compares predictions with flow measurements. A four cylinder 16 valve 1.4 litre gasoline engine was modelled by the 1D engine simulation code, WAVE, from the intake pipe to the tailpipe. Components modelled included the air filter, throttle body, intake plenum, intake manifold, cylinders, exhaust manifold, CCC and two mufflers. WAVE predictions of the engine performance were validated against engine test bed data. Transient exhaust velocities at the cylinder exhaust port were validated under motored conditions using Hot Wire Anemometry (HWA). The CCC was subsequently modelled in 3D using the CFD code STAR-CD. The model included the exhaust manifold, diffuser volume, catalyst monolith, outlet section and outlet pipe. Coupled 1D/3D simulations were then performed at 3000 RPM WOT for both motored and firing conditions. The predicted velocity pulses and the flow distribution across the catalyst monolith were compared with LDA measurements obtained under motored and firing conditions.

1D ENGINE MODELLING

The modelling of the complete engine piping system was performed using the Ricardo WAVE programme [14]. WAVE offers a fully integrated treatment of the time dependent fluid dynamics and thermodynamics by means of a 1D finite difference

formulation to solve the governing compressible flow equations. The specifications of the engine are shown in table 1 and figure 1 (a) shows a schematic of the WAVE model with the entire engine piping system.

Engine type	In-line 4 cylinder
Fuel injection	Multi-point manifold fuel injection
Engine capacity	1388 cc
Bore	76.0 mm
Stroke	76.5 mm
Compression ratio	10.3
Firing order	1-3-4-2
IVO	22 deg BTDC
IVC	62 deg ABDC
EVO	39 deg BBDC
EVC	23 deg ATDC

Table 1. Engine specifications

(a) WAVE model with the whole engine piping system (firing)

(b) WAVE model for the motored engine with exhaust manifold dismantled
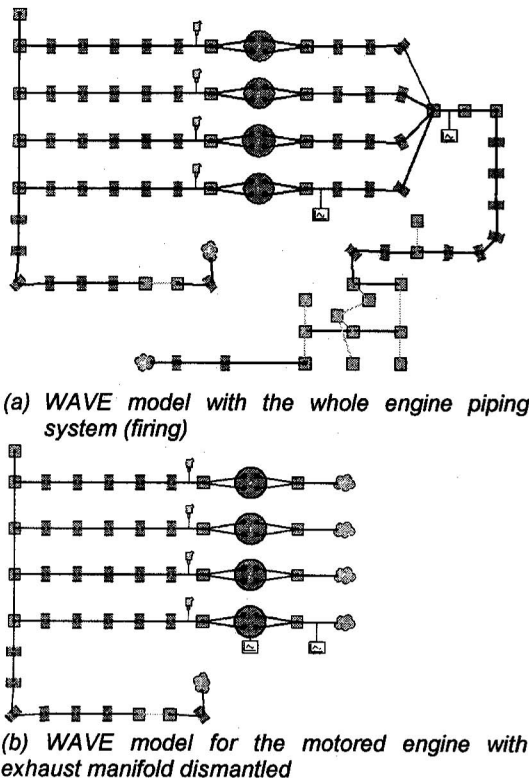
Figure 1. Schematic of the stand-alone WAVE models

To test the accuracy of the WAVE model, simulations were performed under firing conditions, WOT and a wide range of engine speed. Figure 2 compares WAVE predictions with engine test bed data [15]. It can be seen that good agreement was achieved for the volumetric efficiency comparison, with the maximum difference being 6%. As a result, the prediction of the engine brake power and torque was very close to the experimental data. In particular, for engine speeds equal and above 3000 RPM the predictions were within 3% of the engine test results. At low speed the engine may be knock

limited and this may account for the overpredicted power and torque with speeds below 3000 RPM.
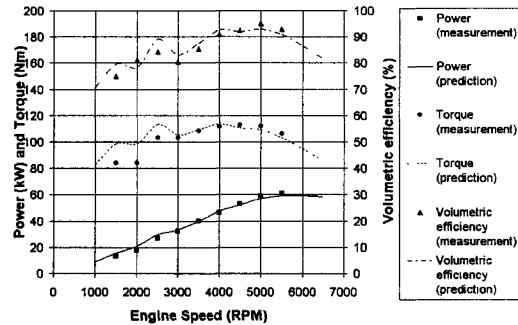
Figure 2. Engine performance validation of WAVE predictions

Since the WAVE model will be subsequently used, in the coupled simulation, to provide boundary conditions for the 3D model of the CCC system, WAVE predictions of the transient exhaust velocity upstream of the exhaust manifold runners (in the exhaust ports) need to be validated. The exhaust manifold (and the piping downstream) was dismantled and the velocity histories were measured along the horizontal and vertical axes at the exit plane of the elliptical exhaust port. The engine was motored under different speeds and loads, and the velocity measurements were obtained using the HWA technique. A corresponding WAVE model was then created, in which the four exhaust ports were directly exposed to the atmosphere since the exhaust manifold was dismantled. Details of the HWA results are presented in [16]. From that study it was shown to be acceptable to treat the flow out of the exhaust port as one-dimensional. Therefore only the velocity traces measured at the centre of the exhaust port were compared with WAVE predictions. The schematic of the WAVE model for the motored engine is shown in figure 1 (b). Figure 3 shows one example of comparing WAVE predictions with HWA measurements. As seen in figure 3 the WAVE prediction matched reasonably well with the experimental data.
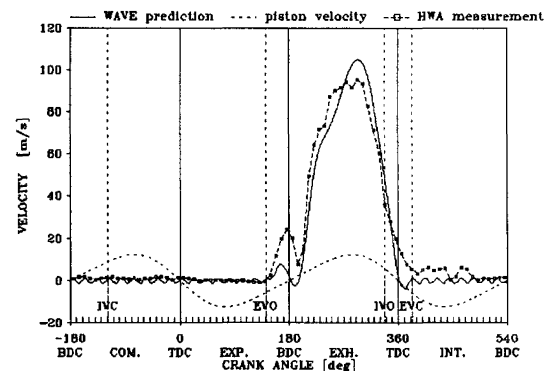
Figure 3. Comparison between the WAVE prediction and HWA measurement at one exhaust port (motored condition, 3000 RPM, WOT)

2

An accurate prediction of the boundary conditions is a prerequisite for the coupled 1D/3D simulations to yield realistic results. The experimental validation of the stand-alone WAVE model described above shows that WAVE is capable of providing fairly accurate boundary conditions for the 3D CFD model.

3D CCC MODELLING

The CCC system was modelled in 3D using the CFD code, STAR-CD [17]. Figure 4 shows the mesh, which contained about 220,000 cells. The 3D model included the exhaust manifold, diffuser volume, catalyst monolith, outlet section and outlet pipe. The runners were extended upstream of the manifold to accommodate optical access for LDA measurements. Another volume for LDA optical access was added between the monolith and the outlet section, in order to measure the velocities downstream of the monolith and provide experimental correlations with the predictions of the co-simulation. To avoid numerical instability in the coupled simulation, the cell layer in the CFD mesh adjacent to the interface between WAVE and STAR-CD was increased in the axial direction.
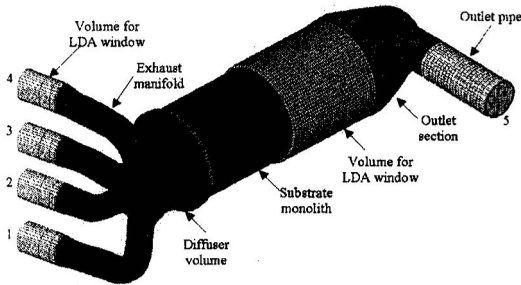
Figure 4. CFD mesh of the CCC system

The inlet plane of the four runners and exit plane of the outlet pipe were defined as five 'inlet boundaries' in STAR-CD. The boundary conditions were provided by user subroutines offered by WAVE. All other surfaces of the CFD mesh were defined as the default 'adiabatic wall'. The PISO algorithm was used for the transient analysis. The time step was equal to $0.5°$ crank angle at 3000 RPM (i.e. 2.7778E-5 s). The second order differencing scheme MARS was used for momentum variables and the first order UD scheme was chosen for turbulence variables and enthalpy. The compressible high Reynolds k-ε model was used as the turbulence scheme and the 'wall function' was used to treat the flow in the wall boundary layer. The density and specific heat of the exhaust gas were provided by WAVE through STAR-CD's user subroutines. The dynamic viscosity and conductivity were defined by polynomial curve fit.

The catalyst monolith was treated as a porous medium in STAR-CD, with the flow resistance formula of the form

$$\frac{\Delta p}{L} = (\alpha|v| + \beta)u \tag{1}$$

where $\Delta p/L$ is the pressure loss per unit length of the monolith channels, u is the superficial velocity in one of the three orthotropic directions, α and β are user-supplied permeability coefficients in that direction and $|\,v\,|$ is the superficial velocity magnitude. Since the flow in the monolith channels is essentially unidirectional, the transverse permeability coefficients were assigned large values (10^8), whilst in the axial direction the channel pressure loss was described by the Hagen-Poisieulle relationship for fully developed laminar flow

$$\frac{\Delta p}{L} = \frac{K\mu}{\varphi d^2}u \tag{2}$$

where K is a constant dependent on the channel cross sectional shape. For ceramic substrates the channel cross section was assumed to be square, hence $K = 28.454$. μ is the dynamic viscosity, variable with temperature, φ is the porosity of the substrate (76%) and d is the channel hydraulic diameter (1.105 mm). In the axial direction, α was defined as zero and β was calculated as in equation (2).

COUPLED SIMULATION

METHODOLOGY

Figure 5 shows the WAVE model in the coupled simulation. WAVE uses special junctions to link with STAR-CD. Each of these junctions was assigned a number (1 to 5) in WAVE, identical to the corresponding boundary number in STAR-CD (see figure 4). WAVE was responsible for starting the co-simulation and ran as the parent programme.
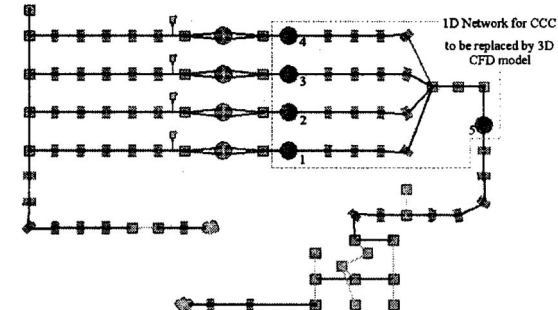
Figure 5. Schematic of the WAVE model in the coupled 1D/3D simulation

The procedure in the coupled simulation takes the following approach.

1. According to the fixed STAR-CD time step, WAVE calculates its own time step size (substepping if required).
2. WAVE solves explicitly the governing equations in its piping system up to the end of a STAR-CD time step.
3. WAVE provides the time averaged flux boundary conditions to STAR-CD, by using STAR-CD's user subroutines.
4. STAR-CD uses WAVE's flux boundary conditions at the end of the time step to solve the flow field in the 3D domain.

5. STAR-CD spatially averages the state boundary conditions and passes them back to WAVE through Ricardo's RSimlink coding.
6. Steps 2 to 5 are repeated for each time step. When the pre-defined simulation time is reached the co-simulation stops.

The coupling methodology requires that the WAVE/STAR-CD connecting interfaces should be flat planes normal to a region of approximately 1D flow. In this study, it is reasonable to treat the flow through the inlet planes of the four exhaust runners and the exit plane of the outlet pipe as one-dimensional. Hence these planes were used as the interfaces between the two codes.

In the WAVE model shown by figure 5, the 1D network linking the 5 special junctions is termed a 'shadow network'. When the shadow network was used, the special junctions to link with STAR-CD were treated no differently from the normal orifice junctions used in WAVE. Hence the WAVE model containing the shadow network in figure 5 was similar to the stand-alone WAVE model in figure 1 (a). The shadow network was replaced by the 3D CFD model in the second phase of the coupled simulation. The purpose in using the shadow network was to reduce the total amount of CPU time required to obtain a converged coupled solution. Therefore in the coupled simulation, WAVE modelled two cases. Case 1 used the shadow network and was run for 20 engine cycles to get a converged solution in WAVE. The flow field was preserved at the end of case 1 and served as the initial flow field in the 1D network in case 2. In case 2 the 1D shadow network was replaced by the 3D STAR-CD model of the CCC system and the two codes performed a coupled simulation using the procedure described above. The preserved flow field in case1 also served as the initial boundary conditions for the STAR-CD model in case 2. Case 2 was run for 3 engine cycles and the results were analysed from the data saved in the last cycle. The co-simulation was performed at 3000 RPM WOT under both firing and motored conditions. The simulations took about 4 and 3 weeks respectively, running on a SGI Octane Unix workstation with a single processor (MIPS R12000) and 2 GB RAM.

SIMULATION RESULTS

Preliminary result analysis

To determine if a converged result is achieved by the coupled simulation, the velocity histories at the centre of runner 1 inlet plane and outlet pipe exit plane in the STAR-CD model were plotted in figure 6 against simulation time for the firing case. As shown, strong boundary fluctuations were observed at the beginning of the coupled run in the first engine cycle. However the velocity histories in the second and third engine cycle did not show much difference. Therefore it was believed that 3 engine cycles were enough for the coupled simulation to converge, and that the third engine cycle produced reliable results.
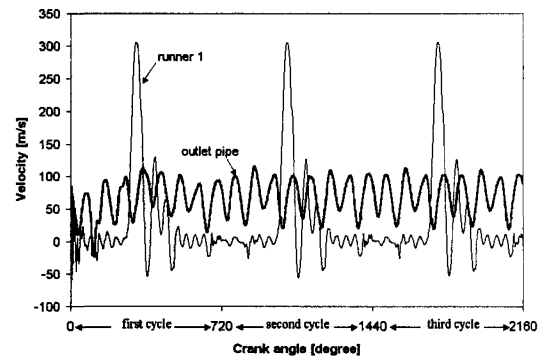
Figure 6. Velocity histories against simulation time (firing engine)

As mentioned earlier, when the 'shadow network' was used in case 1 of the coupled simulation, the solution actually did not include the 3D CFD model. Only when the 'shadow network' was replaced by the 3D CFD model in case 2, the mutual influence between the 1D and 3D codes was realised. Figure 7 shows the velocity history comparisons between the two cases. This shows that incorporating the 3D model modified the boundary conditions at the interface between the two codes.
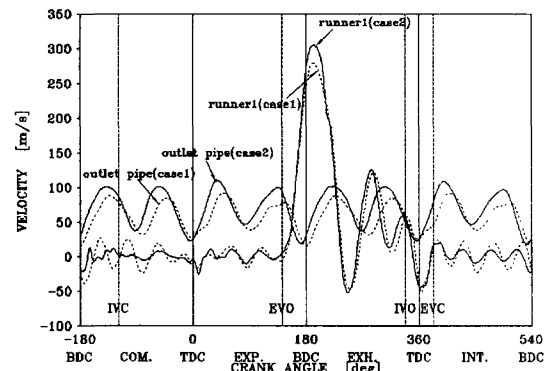
Figure 7. Comparison between two cases in the coupled simulation (firing engine)

Exhaust velocity pulse shapes

Figure 8 shows the comparison between the firing and motored engine predictions of the inlet velocity pulse to runner 1. It can be seen that the pulse shapes were quite different. For the firing case a predominant velocity peak occurred shortly after EVO, which was caused by the 'blow-down' event of the high pressure gas trapped inside the combustion chamber. Two secondary velocity peaks and two reverse flow troughs were also observed between EVO and EVC. It was conjectured that the two secondary peaks were associated with the 'piston displacement' event and pressure harmonics inside the exhaust system. The high 'blow-down' pressure may be partially reflected by the diffuser wall, the front face of the monolith or the closed end of the runner ducts of the other cylinders. These pressure reflections could generate the two reverse flow troughs and could contribute to the generation of the two secondary peaks. Compared with the firing inlet velocity pulse

4

shape, the motored run only showed one 'piston displacement' velocity peak.
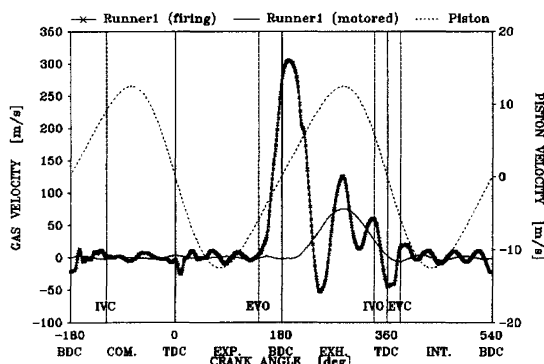
Figure 8. Velocity pulse shape comparison

Experimental correlation

LDA measurements were undertaken in the engine bed tests and the experimental details are given in [16]. One of the optical windows was placed at the far-engine side and ~30 mm downstream of the monolith as shown in figure 10 (a). Data was collected at several locations along the X axis, and the measurement position was defined as distance from the window. Figure 9 shows the spatial and temporal comparisons between LDA measurements and co-simulation predictions of exhaust velocities at different locations. In the temporal comparison (figure 9 (b-f)), four velocity peaks were clearly shown, corresponding to the individual exhaust events of the four cylinders. The predicted velocity pulse shapes and magnitude of the peak flows matched well with LDA in general. In the spatial comparison (figure 9 (a)), the predicted mean velocity profile along the X axis (see figure 10 (a)) exhibited a similar shape to the LDA profile.

Some discrepancies exist between prediction and measurement. In the spatial comparison (figure 9 (a)) for the motored case, the predicted location and magnitude of the max/min velocities are different from experiment. Several factors in the CCC model may affect the accuracy of the predictions of the coupled solution. First, the flow resistance formula in the porous medium region in STAR-CD may be over simplified, as it does not take into account the local resistance increase when the flow impinges on the monolith front face at an oblique angle. This suggests that the pressure loss 'entrance effect' due to oblique entry should be included in the resistance formula in the porous medium [18]. Second, the grid resolution may not be high enough to capture some details in the flow field. Third, the standard k-ε model and 'wall function' boundary layer treatment may not adequately describe the flow field associated with the complex manifold geometry and the highly swirling flow in the diffuser. Fourth, in the firing case the effect of chemical reaction on temperature distribution in the monolith was not considered and the wall was simplified as adiabatic in STAR-CD in both cases. Nevertheless it can be seen that in general fairly good agreement was achieved

between the predictions and LDA for both motored (figure 9 (a-e)) and firing (figure 9(f)) conditions.
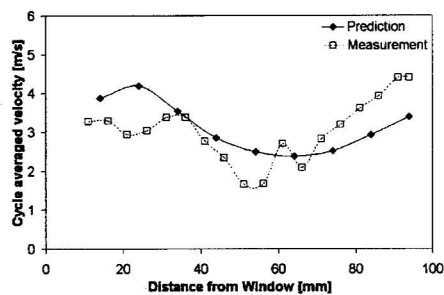
(a) velocity profile comparison (motored engine)
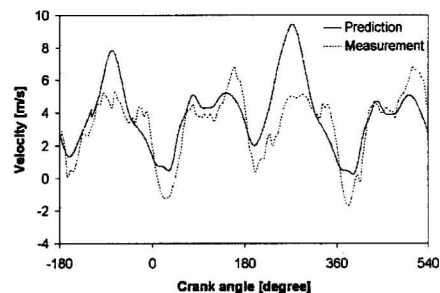
(b) motored engine (~14mm from window)
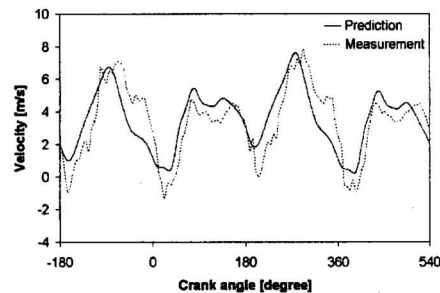
(c) motored engine (~34mm from window)
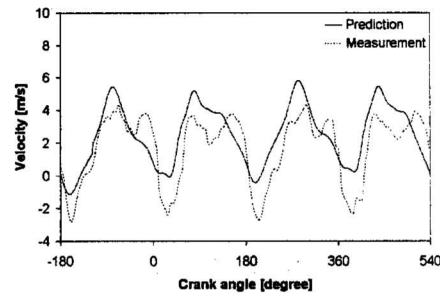
(d) motored engine (~54mm from window)
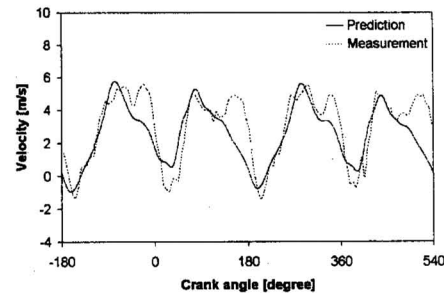
(e) motored engine (~74mm from window)

5
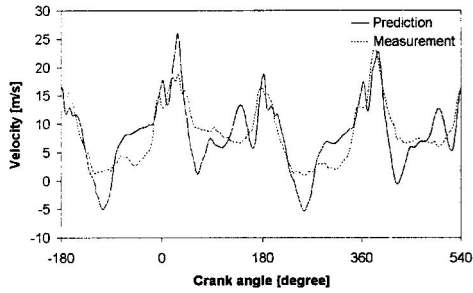
(f) firing engine (~34mm from window)

Figure 9. Velocity comparisons between predictions and LDA downstream of the monolith

Predicted flow maps for firing and motored engine

Different inlet velocities between the firing and motored cases lead to different velocity distributions across the monolith. Figures 10 (b) and (c) show contour plots of the velocity distribution in a circular plane parallel to and ~30 mm downstream of the back face of the monolith for both the firing and motored cases. The velocities were time-averaged over one engine cycle. The view angle is normal to the contour plot plane as shown in figure 10 (a).
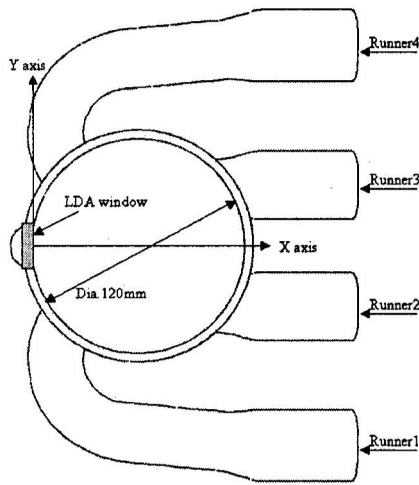
(a) view angle
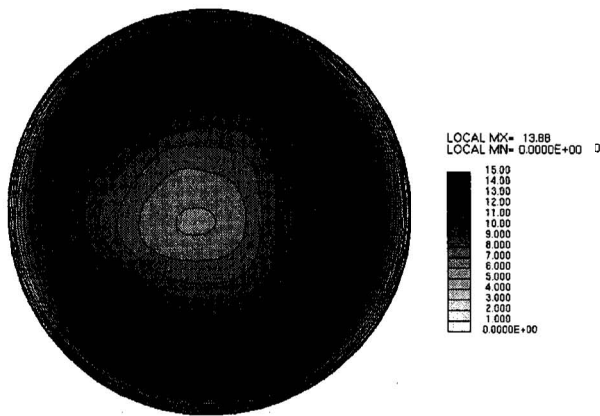
(b) velocity contour plot for the firing engine
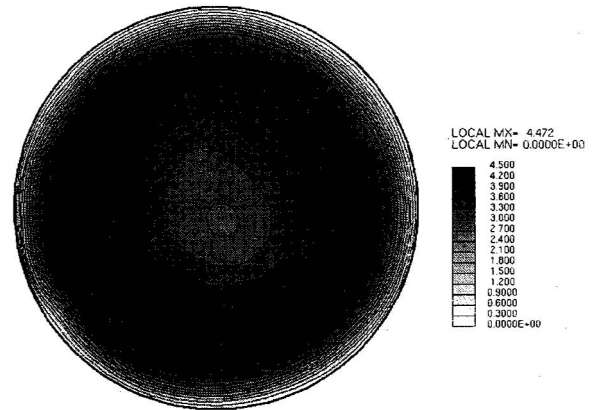
(c) velocity contour plot for the motored engine

Figure 10. Predicted velocity distribution across the monolith

The contour plots in figure 10 (b, c) were not symmetric about the X axis (see figure 10 (a)). This could be due to slight asymmetry in the CFD mesh that was derived from the CAD data of the CCC system. The slight difference in volumetric efficiency of the four cylinders could also worsen the flow symmetry.

The flow distribution in the motored and firing cases shared some common features, namely relatively low velocities in the central and near wall region with an annular region of relatively high velocities in between. For the firing case, the maximum velocity region appeared on both sides furthest from the X axis. However in the motored case, the maximum velocity region appeared on the far-engine side, with a secondary high velocity band on the near-engine side. To reveal the reason for the difference between the two cases, figure 11 shows snapshots at the times of peak flow for the individual cylinder exhaust events for both the firing (left) and motored (right) case. It can be seen that for the firing engine, the high momentum flux of the exhaust gas generated strong swirl. All the four ports thus contributed significantly to the two side regions (furthest from the X axis). When the engine was motored, the momentum flux of the exhaust was much less and the intensity of the swirl was reduced significantly. In this case only ports 1 and 4 contributed to the far-engine side. For these ports the flow was directed by the curvature of the runners and their angles of entry to the diffuser volume. Ports 2 and 3 did not contribute much to the far-engine side due to lower momentum flux. Also the timing of the individual exhaust events was different between the firing and motored cases, as shown in figure 11. This will introduce different port interactions and hence contribute to the velocity distribution differences seen in figure 10 (b, c).

6

port 4 (CA=-151)

port 4 (CA=-78)

port 2 (CA=29)

port 2 (CA=102)

port 1 (CA=209)

port 1 (CA=282)

port 3 (CA=389)

port 3 (CA=462)

Firing engine

Motored engine
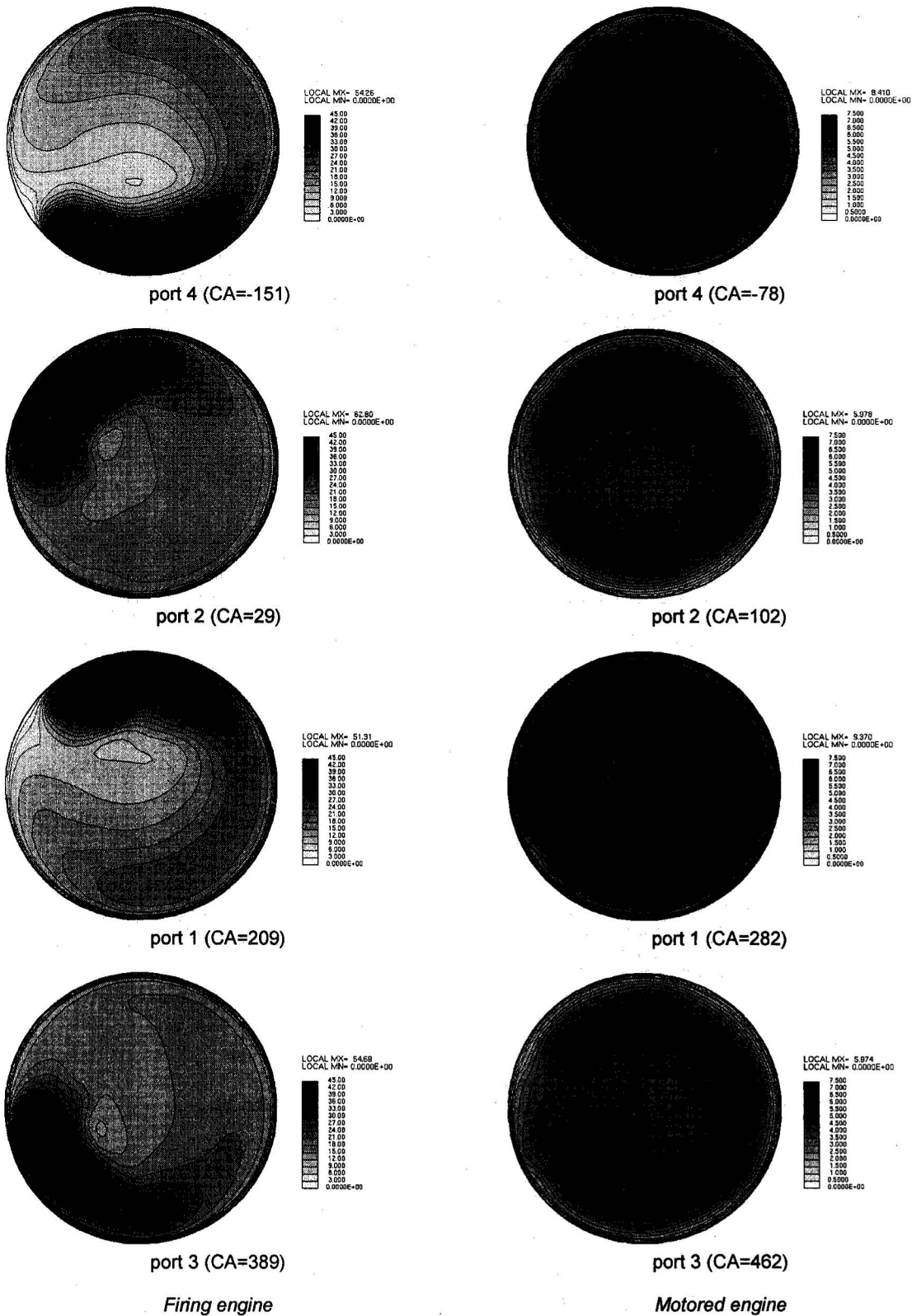
Figure 11. Contour plots of peak flows from individual ports

7

CONCLUSION

The conclusions from this study can be summarised as follows.

1. A co-simulation methodology is introduced which performs coupled solutions between a 1D engine piping system and a 3D CCC model. This hybrid simulation takes into account the mutual influence between the 1D and 3D model.
2. Predictions of exhaust velocities downstream of the monolith matched fairly well with LDA measurements for both motored and firing conditions. This illustrates the potential of using the coupled simulation in the exhaust system design process.
3. The discrepancies between the predictions and measurements suggest further improvement in the 3D CCC model is needed to improve the prediction accuracy of the coupled simulation.
4. The firing and motored engines showed large difference in terms of both the inlet exhaust velocity pulse shapes and the flow distribution across the monolith. This suggests that only the simulation for the firing engine can be utilised to predict the flow distribution across the monolith of a CCC system in a real engine environment.

ACKNOWLEDGMENTS

REFERENCES

1. Benjamin, S. F. and Roberts, C. A., *Warm Up of an Automotive Catalyst Substrate by Pulsating Flow: A Single Channel Modelling Approach,* International Journal of Heat and Fluid Flow 21 (2000) 717-726, 2000
2. Martin, A. P., Will, N. S., Bordet, A., Cornet, P., Gondoin, C. and Mouton, X., *Effect of Flow Distribution on Emissions Performance of Catalytic Converters*, SAE paper 980936, 1998
3. Arias-Garcia, A., Benjamin, S. F., Zhao, H. and Farr, S. *A Comparison of Steady, Pulsating Flow Measurements and CFD Simulations in Close Coupled Catalysts*, SAE paper 01FL-335, 2001
4. Bai, L., Zhao, F. Q., Liu, Y. and Lai, M. C., *Transient Flow and Pressure Characteristics inside a Closed-Coupled Catalyst Converter*, SAE paper 982548, 1998
5. Park, S. B., Kim, H. S., Cho, K. M. and Kim, W. T., *An Experimental and Computational Study of Flow Characteristics in Exhaust Manifold and CCC (Close-Coupled Catalyst),* SAE paper 980128, 1998
6. Lai, M. C., Kim, J. Y., Cheng, C. Y., Li, P., Chui, G. and Pakko, J. D., *Three-Dimensional Simulations of Automotive Catalytic Converter Internal Flow*, SAE paper 915200, 1991
7. Jeong, S. and Kim Taehun, *CFD Investigation of the 3-Dimensional Unsteady Flow in the Catalytic Converter*, SAE paper 971025, 1997
8. Cho, Y. S., Kim, D. S., Han, M., Joo, Y., Lee, J. H. and Min, K. D., *Flow Distribution in a Close Coupled Catalytic Converter,* SAE paper 982552, 1998
9. Payri, F., Benajes, J. and Galindo, J., *One-Dimensional Fluid-Dynamic Model for Catalytic Converters in Automotive Engines*, SAE paper 950785, 1995
10. Zander L. and Bradamante E., *Exhaust System Warm-Up Analysis Using the WAVE Code*, Ricardo Software International User Conference, Detroit, February 1997
11. Weltens, H., Bressler, H., Terres, F., Neumaier H. and Rammoser D., *Optimisation of Catalytic Converter Gas Flow Distribution by CFD Prediction*, SAE paper 930780, 1993
12. Bressler, H., Rammoser, D., Neumaier, H. and Terres, F., *Experimental and Predictive Investigation of a Close Coupled Catalytic Converter with Pulsating Flow*, SAE paper 960564, 1996
13. Berkman, M., Taylor, W. and Ciray, M. S., *1-D/3-D Coupled Transient CFD Analysis of a Hot-End Automotive Exhaust System*, Proceeding of ASME FEDSM2001- 18206, New Orleans, USA, May29-June01, 2001
14. Ricardo Inc., *User's Manual for Ricardo WAVE*, version 3.6, June 2001
15. Liu, Z., *Pulsating Flow Maldistributon in Exhaust Catalyst – the Effect of Pulse Shape and Substrate Resistance*, MPhil/PhD transfer report, Coventry University, 2002
16. Arias-Garcia, A., *Investigation of the Flow Performance of Automotive Close Coupled Catalyst on Flow Rigs and Engines*, PhD thesis, Coventry University, 2002
17. Computational Dynamics Ltd, *STAR-CD Users Guide and Methodology (version 3.15)*, 2001
18. Benjamin, S. F., Haimad, N., Roberts, C. A. and Wollin J., *Modelling the Flow Distribution Through Automotive Catalytic Converters*, Proc. Instn. Mech. Engrs. Vol. 215 Part C, 2001

CONTACT

Prof S. F. Benjamin
Coventry University
School of Engineering
Priory Street, Coventry
CV1 5FB, United Kingdom
Email: s.benjamin@coventry.ac.uk

NOMENCLATURE AND ABBREVIATION

Δp	Pressure loss
L	Channel length in the catalyst monolith
$\lvert v \rvert$	Superficial velocity magnitude
u	Superficial velocity
α, β	Permeability coefficients
K	Constant
d	Channel hydraulic diameter
μ	Dynamic viscosity
φ	Porosity of catalyst substrate

k Turbulent kinetic energy
ε Turbulent kinetic energy dissipation rate

CA   Crank Angle
CCC   Close Coupled Catalyst
CFD   Computational Fluid Dynamics
EVO   Exhaust Valve Opening
EVC   Exhaust Valve Closing
HWA   Hot Wire Anemometry
IVO   Intake Valve Opening
IVC   Intake Valve Closing
LDA   Laser Doppler Anemometry
RPM   Revolutions Per Minute
SI   Spark Ignition
WOT   Wide Open Throttle